MATHEMATICAL BIOSCIENCES
AND ENGINEERING
Volume **13**, Number **3**, June **2016**

doi:10.3934/mbe.2016001

pp. **461–481**

THE EFFECT OF POSITIVE INTERSPIKE INTERVAL CORRELATIONS ON NEURONAL INFORMATION TRANSMISSION

Sven Blankenburg and Benjamin Lindner

Bernstein Center for Computational Neuroscience Berlin
Berlin 10115, Germany
and
Department of Physics, Humboldt-Universität zu Berlin
Berlin 10099, Germany

Abstract. Experimentally it is known that some neurons encode preferentially information about low-frequency (slow) components of a time-dependent stimulus while others prefer intermediate or high-frequency (fast) components. Accordingly, neurons can be categorized as low-pass, band-pass or high-pass information filters. Mechanisms of information filtering at the cellular and the network levels have been suggested. Here we propose yet another mechanism, based on noise shaping due to spontaneous non-renewal spiking statistics. We compare two integrate-and-fire models with threshold noise that differ solely in their interspike interval (ISI) correlations: the renewal model generates independent ISIs, whereas the non-renewal model exhibits positive correlations between adjacent ISIs. For these simplified neuron models we analytically calculate ISI density and power spectrum of the spontaneous spike train as well as approximations for input-output cross-spectrum and spike-train power spectrum in the presence of a broad-band Gaussian stimulus. This yields the spectral coherence, an approximate frequency-resolved measure of information transmission. We demonstrate that for low spiking variability the renewal model acts as a low-pass filter of information (coherence has a global maximum at zero frequency), whereas the non-renewal model displays a pronounced maximum of the coherence at non-vanishing frequency and thus can be regarded as a band-pass filter of information.

1. **Introduction.** Neurons encode time-dependent sensory signals in sequences of action potentials, so-called spike trains. How the nonlinear and stochastic (noisy) dynamics of the neuron shapes this encoding process is an active topic of current research in computational neuroscience. Many nerve cells fire spikes already in the absence of sensory stimulation — they are spontaneously active. How do the properties of this spontaneous activity influence their signal transmission capabilities if a stimulus is presented to the neuron? This very general question has been addressed, for instance, for neurons that show a pronounced *non-renewal* spontaneous spiking, i.e. their spike trains display correlations among the intervals between adjacent spikes (so-called interspike intervals or short ISIs). It has been demonstrated that negative ISI correlations can significantly enhance the transmission of a broad-band

2010 *Mathematics Subject Classification.* 93E03, 93E11, 94A12, 94A15, 94A24, 60G10, 60G15, 60G35, 60G50, 60G55.

Key words and phrases. Stochastic neuron models, non-renewal point process, neural signal transmission, information filtering.

signal [10, 12, 9], an idea that may be also usable for artificial signal detectors [37]. ISI correlations can arise for various reasons and can be different in sign, shape, and function.

Besides the total amount of transmitted information, the neural encoding of specific stimulus features may be also worth to be investigated. A number of experimental and theoretical studies explored, how the signal transmission of certain neural systems differs for the slow, intermediate and fast components of a time-dependent signal. This can be quantified by the spectral coherence function, a frequency-dependent correlation coefficient between zero and one, which has been measured, for instance, in the vestibular system of monkey [43, 33], the auditory system of bullfrog [40] and cricket [32], and the electrosensory system of electric fish [11, 35, 36]. By means of high values of the coherence at low, intermediate or high frequencies we can distinguish low-pass, band-pass, and high-pass filters of information. For a more faithful measure of information filtering, see the frequency-resolved mutual information rate recently suggested by [3].

Features of the dynamics that shape the neural information filter have also received some attention from theoreticians. First of all, the simplest yet not completely unrealistic neuron model, the integrate-and-fire (IF) neuron with white background noise, transmits most information about slow components of a broadband stimulus [51, 27]. Remarkably, this low-pass filter property is independent of the firing regime (tonic, irregular, or bursting) and the kind of subthreshold nonlinearity that distinguishes different (perfect, leaky, and quadratic) IF neurons. This raises the question by which mechanisms a pronounced band-pass or high-pass information filter may arise.

An additional source of high- or low-pass filtering may originate in short-term synaptic plasticity [52, 1]. Although we do not observe this with a homogeneous population of synapses that are all facilitating or all depressing [29, 34], the picture changes if we take into account that most cortical neurons receive different signals through subpopulations of either depressing or facilitating synapses (heterogeneous synaptic short-term plasticity). Specifically, information on stimuli that arrive through depressing synapses may be high-pass filtered [15]. Another mechanism for low- and high-pass filtering of information is associated with bursting in cells with active dendrites [38]. Sorting spikes from cells with active dendrites into bursts and isolated spikes, one finds that the latter code for high-frequency bands, whereas bursts have a large coherence at low frequencies only - a result that was first observed experimentally in pyramidal cells in weakly electric fish [38]. A third mechanism for information filtering at the cellular level is observed for neuron models that display pronounced subthreshold oscillations due to the presence of slow ionic currents [25, 8, 16]. Variants of the resonate-and-fire neuron show band-pass filtering of information [4]. Finally, at the population level it has been shown that synchronous spikes of neurons, which are stimulated by a common signal, carry more information about high than about low frequencies [46] confirming and explaining earlier experimental findings [35].

In this paper we suggest a new and simple mechanism for a band-pass filtering of information about a broad-band stimulus. This is based on positive ISI correlations in the neuron's spontaneous activity. Such correlations are experimentally observed (see e.g. [30, 17]) and can originate from an slow external stimulus [26], slow intrinsic channel noise [44], or subthreshold spike-frequency adaptation [39, 47]. We explore the consequences of a positive ISI correlation for the frequency-resolved information

transmission in two analytically tractable neuron models. The two models are similar in their spontaneous spiking and their linear response but differ only in their ISI correlation: the renewal model generates a spike train with independent ISIs while the non-renewal model displays a positive correlation between adjacent ISIs. This comparison of non-renewal and renewal models is similar in spirit and analytical methodology to the studies by [12] and [28] that explored the effect of negative ISI correlations on neural signal transmission.

Our paper is organized as follows. We start by introducing the models and measures of interest, explain then how the latter can be calculated or at least approximated analytically, compare our results to numerical simulations of the model, and discuss the noise-shaping effect that leads to band-pass filtering of information. Details of the calculations are presented in the appendix.

2. Models and measures.

Here we introduce the simple perfect integrate-and-fire models with threshold noise by means of which we will investigate the effect of positive ISI correlations on neural signal transmission. We will also define the measures of interest and give analytical expressions or at least approximations for these statistics.

2.1. Neuron model.

For both models, the input is integrated according to

$$\frac{dv}{dt} = \mu + s(t), \tag{1}$$

where $v(t)$ is the membrane voltage and μ is a constant base current, which we choose in the following as $\mu = 1$ (all parameters are given in non-dimensional units, including time-scales and frequencies); $s(t)$ is the input signal discussed below. As in all IF models upon reaching a threshold v_T the voltage is reset to a value v_R and the i-th spike time t_i is registered. The models are illustrated in Fig. 1 in the absence of a stimulus ($s(t) \equiv 0$, spontaneous activity). In our setup v_T and v_R are not fixed but vary stochastically from spike to spike as follows. For both models we draw after each spike a random threshold v_T from an inverse Gaussian distribution $P_T(v_T)$ in the range $[0, \infty]$; for the specific distribution, see below Eq.(6). The two models differ in the generation of the reset value v_R. For the *renewal* model v_R is drawn from a mirrored distribution of negative values, i.e. $p_R(v_R) = p_T(-v_R)$, see below Eq.(6). All random values of threshold and reset are statistically independent in this model and this leads to ISIs that are also completely independent of each other (see Fig. 1d). in

For the *non-renewal* model we use the preceding threshold value (i.e. v_T mirrored along zero) as the next reset value. This leads to the same statistical distribution of reset values as in the renewal model. Moreover, a high value of the threshold (implying a preceding ISI which is larger than the mean ISI on average) causes a low value of the following reset (implying a subsequent ISI that is likewise larger than the mean ISI on average). So the particular reset rule leads to a positive correlation between adjacent intervals with a serial correlation coefficient of 1/2 (see Fig. 1d and appendix, sec. (4)).

Although random fluctuations of a firing threshold have been observed in experiments [2, 9] and used in theory [20, 12] we do not claim that our models with their stochastic threshold and reset values capture the subthreshold membrane voltage of real neurons. Rather our two models are intended to describe features of real neurons' spike train statistics in an analytically tractable manner. Moreover, because

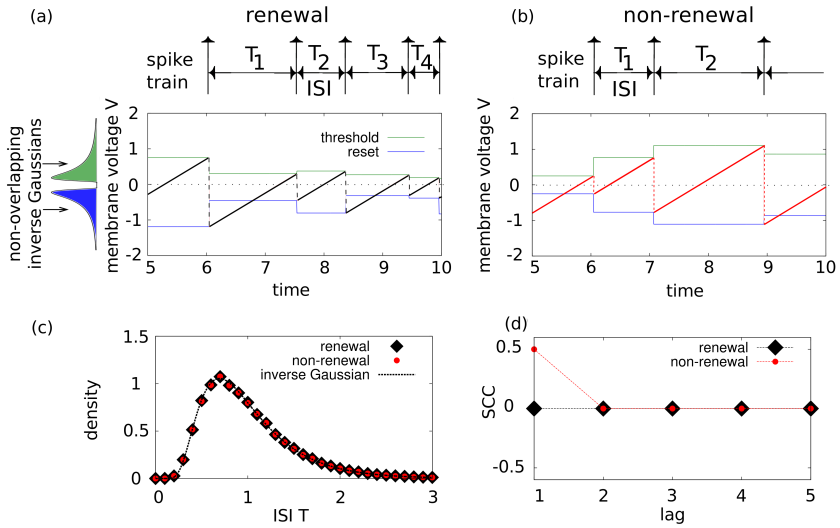

FIGURE 1. **Spontaneous activity of the two models studied in this paper.** Time course of the membrane voltage of the integrate-and-fire model with threshold noise in the renewal version (a) and the non-renewal version (b). In the renewal model (a) the threshold (green) and reset (blue) values are drawn independently from an inverse Gaussian distribution (indicated on the top left and given in Eq.(5)). In the non-renewal model (b) each reset value is a flipped version of the previous threshold value (which is mirrored along the time axis), giving rise to positive correlations between adjacent ISIs (d). Both models display exactly the same ISI distribution (c) (see Eq.(5) below) which is an inverse Gaussian though with different mean and variance than the ones used for threshold and reset.

of their simplicity, renewal and non-renewal versions differ exactly in one statistical property only, the interval correlation, and are thus amenable to a quantitive comparison of their signal transmission characteristics (see below). With our choice of the inverse Gaussian probability density for the values of threshold and reset, the ISI density will be an inverse Gaussian as well. This function coincides with the ISI density of a perfect integrate-and-fire model driven by white Gaussian noise, which is one of the classical results in theoretical neuroscience [21]. Typically, the inverse Gaussian probability density is a unimodal distribution skewed to the right that displays a suppressed probability at very short intervals (reflecting a refractory state) and possesses a pronounced tail describing the distribution of long intervals. These features are shared by the ISI histograms of many neurons (see, for instance, [6]); indeed, the ISI density of some neurons can be well fit by an inverse Gaussian [21, 17].

If we switch on a signal $s(t)$ it will modulate the speed with which the voltage approaches the threshold and will thus affect the spike times generated by the model. In this way, the signal will be encoded in the sequence of spikes. It is the central question of this paper how the positive ISI correlations in the non-renewal

model influence the transmission of the signal $s(t)$. For the signal $s(t)$ we will use a band-limited Gaussian white noise with a variance $\langle s^2 \rangle = \varepsilon^2$ and a cut-off frequency f_c. The power spectrum of such a stimulus is given by

$$S_{\mathrm{st}}(f) = \frac{\varepsilon^2}{2f_c}\Theta(f - f_c), \tag{2}$$

where $\Theta(f)$ is the Heaviside function. Note that our model includes two kinds of stochasticity (randomness): the random values of threshold and reset describe in a simplified manner intrinsic neural variability, whereas the randomness of the external stimulus is a simple model for a complex time-dependent sensory signal.

2.2. **Spike train statistics and spectral measures.** Using the spike times t_i given by the threshold crossings we can define a spike train for the associated point-process [22]:

$$x(t) = \sum_i \delta\left(t - t_i\right). \tag{3}$$

An important characteristics of neural variability is the statistics of the interspike interval (ISI), $T_i = t_i - t_{i-1}$. The time averaged firing rate r and the coefficient of variation (CV) of the ISI can be both expressed by the first two moments of the ISI as follows

$$r_0 = \frac{1}{\langle T_i \rangle_i}, \quad C_{\mathrm{V}} = \frac{\sqrt{\langle (T_i - \langle T_i \rangle_i)^2 \rangle_i}}{\langle T_i \rangle_i}, \tag{4}$$

where $\langle \ldots \rangle_i$ means an average performed over the index i. If the C_{V} is zero then the spike-train $x(t)$ is regular (pacemaker cell), whereas a C_{V} around one indicates a more irregular spike train, similar to a Poisson process. For comparison, the C_{V} for the spike trains in Fig. 1 is $C_{\mathrm{V}} = 0.5$.

Instead of only measuring the mean and the variance of the ISI we can also ask for the probability density $F_1(T)$ of the single ISI T (where we drop the index). Fortunately, for our simple models and by construction we know the ISI density of the spontaneous activity exactly. If the reset and threshold values are distributed according to inverse Gaussian probability distributions, the ISI is a sum of two independent random variables that are likewise distributed according to such probability distributions. This is so because without additional signal the voltage having constant speed translates random voltage differences between reset and threshold into random time intervals (ISIs) with similar distributions. The voltage started at the reset point goes to zero in a first time interval, $\hat{\tau}_i$ distributed according to $F_{\mathrm{IG}}(\hat{\tau}_i)$, and continues from zero to the threshold value in a second time interval, τ_i, also distributed according to $F_{\mathrm{IG}}(\tau_i)$. Now, the sum of two intervals, both distributed according to the same inverse Gaussian function, is likewise distributed according to an inverse Gaussian, though with mean and variance doubled, compared to the single intervals, $\hat{\tau}_i, \tau_i$, [18].

The inverse Gaussian distribution of the ISI can be conveniently parameterized in terms of the inverse mean value, i.e. the firing rate r_0, and the coefficient of variation C_{V}

$$F_1(T) = \sqrt{\frac{1}{2\pi r_0 C_{\mathrm{V}}^2 T^3}} \exp\left[-r_0 \frac{(T - 1/r_0)^2}{2C_{\mathrm{V}}^2 T}\right]. \tag{5}$$

Using the above discussed relation between threshold and reset distributions on the one hand and the ISI distribution on the other hand, we can prescribe C_V and

rate of the output spike train by drawing the threshold and reset values from the following distributions

$$p_{\mathrm{T}}(v_T) = \sqrt{\frac{\mu}{8\pi r_0 C_{\mathrm{V}}^2 v_T^3}} \exp\left[-r_0 \frac{\left(v_T - \mu/\left(2r_0\right)\right)^2}{2C_{\mathrm{V}}^2 v_T \mu}\right], \quad p_{\mathrm{R}}(v_R) = p_{\mathrm{T}}(-v_R). \tag{6}$$

For the renewal model we have to draw the reset values from the mirrored distribution $p_{\mathrm{R}}(v_R)$. In the non-renewal model the reset values are determined by mirroring the respective preceding threshold value, leading to the very same statistical distribution of reset values as in the renewal model. For all parameter sets studied in this paper the mean values of the two distributions for threshold and reset are set to $1/2$ such that with $\mu = 1$, the firing rate is always one, $r_0 = 1$.

In order to characterize the statistical dependence among the ISIs, we use the serial correlation coefficient (SCC)

$$\rho_k = \frac{\langle (T_{i+k} - T_i)\left(T_i - \langle T_i\rangle_i\right)\rangle_i}{\langle \left(T_i - \langle T_i\rangle_i\right)^2\rangle_i}. \tag{7}$$

The SCC of the spontaneous spiking activity (without signal, i.e. $s(t) \equiv 0$) for the renewal model is zero for higher lags than zero, because all threshold and reset values are independent from each other, and thus the corresponding intervals are independent as well, implying

$$\rho_{\mathrm{R,k}} = 0, \qquad k > 0. \tag{8}$$

This is different for the non-renewal model for which each reset value equals the negative image of the foregoing threshold value. As outlined above, a high (low) threshold value implies a long (short) foregoing ISI which is then, by virtue of the low (high) reset value, followed by a longer (shorter) subsequent ISIs. As shown in the appendix, sec. (4), this leads to a pronounced positive correlation exclusively between adjacent ISIs

$$\rho_{\mathrm{NR,k}} = \frac{1}{2}\delta_{1,k}, \qquad k > 0. \tag{9}$$

To study the signal transmission of the neuron models in the framework of Shannon's information theory [45, 13], we will work in the following in the frequency domain. Let $x(t)$ be the output spike train of the neuron subjected to the signal $s(t)$. The Fourier transform of a stochastic process will be denoted by a tilde and is for a finite time window $[0, T]$ defined as

$$\tilde{x}_T(f) = \int_0^T dt\, e^{2\pi i f t} x(t), \tag{10}$$

Given the output spike train $x(t)$ and the signal $s(t)$, the power spectrum of $x(t)$ and the input-output cross-spectrum are given by

$$S_{x,x}(f) = \lim_{T\to\infty} \frac{\langle \langle \tilde{x}_T(f)\tilde{x}_T^*(f)\rangle_{v_T,v_R}\rangle_s}{T}, \tag{11}$$

$$S_{x,s}(f) = \lim_{T\to\infty} \frac{\langle \langle \tilde{x}_T(f)\tilde{s}_T^*(f)\rangle_{v_T,v_R}\rangle_s}{T}, \tag{12}$$

Here the star denotes the complex conjugated and the average is performed both with respect to the internal noise and the external stimulus.

The spike train power spectra in the spontaneous case (renewal or non-renewal) can be given in terms of the Fourier transforms of the probability density of the n-th order interval $T_{\rm n}$, $F_n = F(T_{\rm n})$ [24]

$$S_0(f) = r_0 \left(1 + \sum_{n=1}^{\infty} \tilde{F}_n(f) + \tilde{F}_n^*(f) \right). \tag{13}$$

In case of a renewal process we have that $\tilde{F}_n(f) = \left(\tilde{F}_1(f)\right)^n$. In the absence of a signal (which we indicate in the following by the index "0"), we thus obtain the well-known formula [50]

$$S_{\rm R,0}(f) = r_0 \frac{1 - |\tilde{F}_{1,0}(f)|^2}{|1 - \tilde{F}_{1,0}(f)|^2} = r_0 \frac{1 - \tilde{F}_{1,0}(f)\tilde{F}_{1,0}(-f)}{\left(1 - \tilde{F}_{1,0}(f)\right)\left(1 - \tilde{F}_{1,0}(-f)\right)}, \tag{14}$$

where we used that $\tilde{F}_{1,0}^*(f) = \tilde{F}_{1,0}(-f)$.

For the nonrenewal model studied here we have that $\tilde{F}_n(f) = \tilde{F}_\tau^2(f)\tilde{F}_\tau(2f)^{n-1}$, where $\tilde{F}_\tau(f)$ denotes the characteristic function of the probability density of threshold and reset values (see sec. (4)). The expression for the spontaneous power spectrum of the spike train can be significantly simplified (see the appendix, sec. (4)) and reads

$$S_{\rm NR,0}(f) = r_0 \frac{\left|1 - \sqrt{\tilde{F}_{1,0}(2f)}\right|^2 + 2\Re\left[\tilde{F}_{1,0}^*(f)\left(1 - \sqrt{\tilde{F}_{1,0}(2f)}\right)\right]}{|1 - \sqrt{\tilde{F}_{1,0}(2f)}|^2}, \tag{15}$$

where $\Re[...]$ denotes the real part of a complex number. We conclude that for calculating the power spectra of both models in the spontaneous case ($s(t) \equiv 0$), we need to know only the characteristic function of the ISI. For an inverse Gaussian ISI density, this function is known and reads:

$$\tilde{F}_{1,0}(f) = \exp\left(\frac{1}{C_{\rm V,0}^2} \left(1 - \sqrt{1 - 4\pi i f \frac{C_{\rm V,0}^2}{r_0}} \right) \right), \tag{16}$$

The cross-spectrum between input signal, $s(t)$, and evoked output spike train, $x(t)$, can be written in terms of the power spectrum of the input signal

$$S_{x,s}(f) = \chi(f) S_{st}(f) = \frac{r_0}{\mu} S_{st}(f). \tag{17}$$

In the last step we have used that the susceptibility $\chi(f)$ of the perfect IF model with threshold noise is a constant with respect to frequency, i.e. $\chi = r_0/\mu$ [28].

The spike-train power spectrum in presence of a weak broadband stimulus can be approximated by this following simple expression (theory I from [28]):

$$S_{\rm I}(f) = S_0(f) + |\chi(f)|^2 S_{\rm st}(f) = S_0(f) + \frac{r_0^2}{\mu^2} S_{st}(f). \tag{18}$$

For a *linear* system, the first formula would be exact, i.e. the power spectrum of the driven system equals the sum of the power spectrum of the unperturbed system (here denoted by $S_0(f)$) and the transmitted signal power (here described by the susceptibility $\chi(f)$ and the signal spectrum $S_{\rm st}(f)$). Applying the formula to a nonlinear system is an approximation of unknown accuracy. Nevertheless, it has

been widely used in the literature on nonlinear stochastic systems with external driving (for an in-depth discussion and references, see [28]).

For the perfect IF model with threshold noise and external driving, an alternative theory for the power spectrum (in the following called theory II) has been developed by [28]. It turns out that the following formula can be applied in our setup as well:

$$S_{\mathrm{II}}(f) = r_0 + |\chi(f)|^2 S_{\mathrm{st}}(f) + \int_{-\infty}^{\infty} df' \, (S_0(f') - r_0) \, I(f, f'), \tag{19}$$

$$\begin{aligned} I(f, f') &= \frac{4 \left(a f'^2\right)^3}{\left[a^2 f'^4 + 4\pi^2 \left(f - f'\right)^2\right]^2} \\ &+ 2\Re \left[\frac{\left(a f'^2 - 2i\pi f\right)^2}{\left[a f'^2 - 2i\pi \left(f - f'\right)\right]^2} \int_{-\infty}^{\infty} d\tilde{f} \frac{S_{\mathrm{st}}\left(\tilde{f}\right)/\mu^2}{a f'^2 - 2i\pi \left(f - f' - \tilde{f}\right)} \right], \end{aligned} \tag{20}$$

with the abbreviation $a = \pi^2 \varepsilon^2 / (f_c \mu^2)$. Theory II is valid for a weak noise only but still captures nonlinear effects of the signal on the power spectrum. It can, for instance, quantitatively describe how a band-pass limited signal (having power only up to a cut-off frequency f_c) broadens a spectral peak that is outside the signal band, e.g. a peak at $f > f_c$.

The derivation of the formulas above is a nontrivial matter but works, briefly, as follows. The system with driving signal ($\dot{v} = \mu + s(t)$) can be mapped to the spontaneous system $\dot{v} = \mu$ by a nonlinear time transformation. A necessary condition for a unique mapping (a monotonic time transformation) is that $\sqrt{\langle s^2 \rangle} \ll \mu$ (weak signal amplitude). Then, using i) the Wiener-Khinchin theorem, ii) the relation between the conditional spike counts of the driven and the spontaneous system, iii) a Markovian approximation for a needed conditional average of the signal and iv) a number of manipulations of the resulting integral expressions in the Fourier domain, gives the final result stated above in Eq.(19) and Eq.(20).

Information transmission in our setup can be studied by using the spectral coherence function [41, 42]

$$C(f) = \frac{|S_{x,s}(f)|^2}{S_{x,x}(f) S_{s,s}(f)}. \tag{21}$$

The coherence function is a correlation coefficient, which is restricted to $[0, 1]$ and measures which spectral components of the input are represented in the output. A value of the coherence close to one at a certain frequency indicates that the output carries almost all information of this spectral component of the stimulus, whereas a value close to zero implies that almost no information is linearly encoded about the signal component in this frequency band. Thus, the coherence can be regarded as an approximate measure of information filtering.

Using theory I for the power spectrum, the coherence function between evoked output spike train and input signal can be approximated by

$$C_I(f) = \left[1 + \frac{2 f_c \mu^2 S_0(f)}{r_0^2 \varepsilon^2}\right]^{-1}, \tag{22}$$

which we will use below to study the shape of the coherence function analytically. We will also compare the coherence, using Eq.(21) and the power spectrum of theory II, Eq.(19), to numerical simulations.

One possible measure of the extent of band-pass filtering of information is

$$Q = C(\hat{f})/C(0), \tag{23}$$

where $\hat{f}$ denotes the frequency at which the coherence attains its global maximum. Clearly, for a low-pass filter of information, we have $Q = 1$, whereas values significantly larger than one indicate a band-pass or high-pass filter.

By means of the coherence function we can also estimate the total amount of transmitted information using a lower bound formula for the mutual information rate

$$\mathcal{M}_{\mathrm{LB}} = -\int_0^\infty df \log_2 (1 - C_{\mathrm{SR}}(f)). \tag{24}$$

This formula has been proven mathematically in Ref. [19]; for a number of instructive examples in the neurobiological context, see the review by [5], for a recent study of how tight this bound is in case of a leaky integrate-and-fire model, see [3]. We note that for the models studied here the integral in Eq.(24) has to be evaluated numerically.

3. **Results.** Here we present the theoretical predictions for the spectral measures and compare them to results of stochastic simulations of the two models. We will vary the signal strength and the intrinsic variability of the model neuron, which is parameterized solely by the CV of the spontaneous activity. Note that the latter is generally smaller than the CV of the evoked activity (both are compared below in Fig. 6). Because the perfect IF neuron is commonly used to model rather regular spiking behaviour of tonically firing cells (see e.g. the studies by [21] and [17]) with $C_{\mathrm{V}} \leq 0.5$, we restrict ourselves in this study to this regime of low CV of the spontaneous activity.

3.1. **ISI correlations lead to band-pass-filtering of information.** Before we systematically explore the dependence of spectra and coherence on system parameters, let us highlight the main effect of positive ISI correlations on signal transfer, i.e. the main difference between the renewal and the non-renewal models. In Fig. 2 we show the squared cross-spectra between input and output, the spike train power spectra, and the coherence functions of the two models. While there is no difference in the cross-spectra (Fig. 2a), the power spectra of the two models (Fig. 2b) differ significantly due to the noise-shaping effect of positive correlations: the non-renewal model has more power at low frequencies but reduced power in an intermediate frequency range about $f \approx 1/2$, corresponding to half of the firing rate, $r_0 = 1$. This effect can already be understood from the inspection of the spontaneous power spectra, which is for the case shown close to the spectrum according to theory I, Eq.(18) (dashed lines in Fig. 2b). Generally, we know that the spike train power spectrum of a stationary point process obeys the relation [14]

$$S(0) = r_0 C_{\mathrm{V}} \left(1 + 2 \sum_{k=1}^{\infty} \rho_k \right). \tag{25}$$

Both models have the same rate and C_{V}, implying that

$$S_{\mathrm{NR}}(0) = r_0 C_{\mathrm{V}} (1 + 2\rho_1) = 2 r_0 C_{\mathrm{V}} = 2 S_{\mathrm{R}}(0) \tag{26}$$

because in the renewal model $\sum_{k=1}^{\infty} \rho_k = 0$. Thus, the non-renewal model has twice as much power at low frequencies as the renewal model, which is only slightly

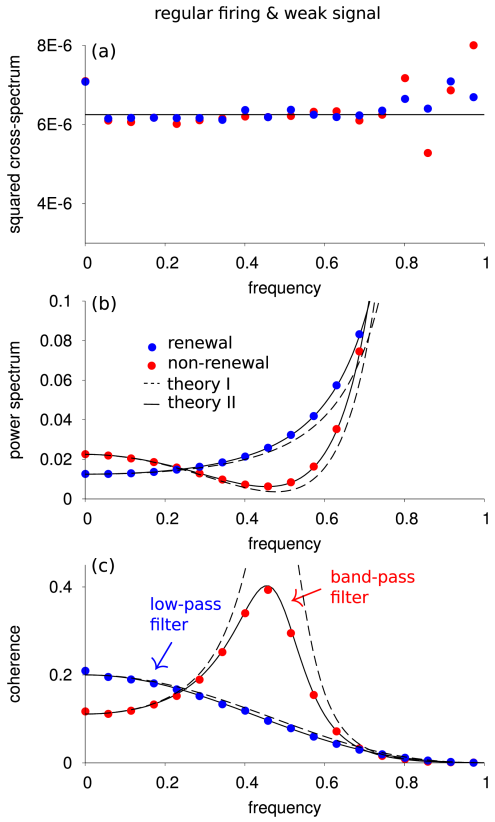

FIGURE 2. **Information filtering of the two models.** Numerical results (symbols) compared to theory I (dashed lines) and theory II (solid lines) for $C_{\mathrm{V},0} = 0.1$ of the spontaneous activity and a weak input signal $s(t)$ ($\varepsilon^2 = 0.01$). Theory I predicts a maximum of the coherence at much higher values ($C \approx 0.7$), which is not shown.

changed by the presence of a weak signal (cf. Fig. 2b). Because the total integral over the power spectra is unchanged (for the same reason given by [12] and [28] for the IF neuron with negative ISI correlations), the increased power at low frequencies has to be reduced in some other frequency range, an effect known as noise shaping [49, 48, 31]. Fig. 2b reveals that this reduction is observed at intermediate frequencies around half of the firing rate (for our numerical example, $f = r_0/2 = 1/2$). We recall that the coherence is essentially the ratio between squared cross-spectrum and power spectrum (cf. Eq.(21)). Hence, we can conclude that the coherence function of the non-renewal model must have a pronounced peak at the intermediate range about $f \approx 1/2$ but is small at low frequencies, which is indeed what we observe in Fig. 2c. The renewal model, in contrast, shows a low-pass coherence function, similar to standard IF models with more realistic intrinsic current noise [51].

Both theory I and II capture this band-pass filtering of information qualitatively. However, because the intrinsic noise for the example is quite low, we are not completely in the linear response regime and thus the quantitative agreement of theory I with the simulated coherence is not good around its maximum. In contrast, theory

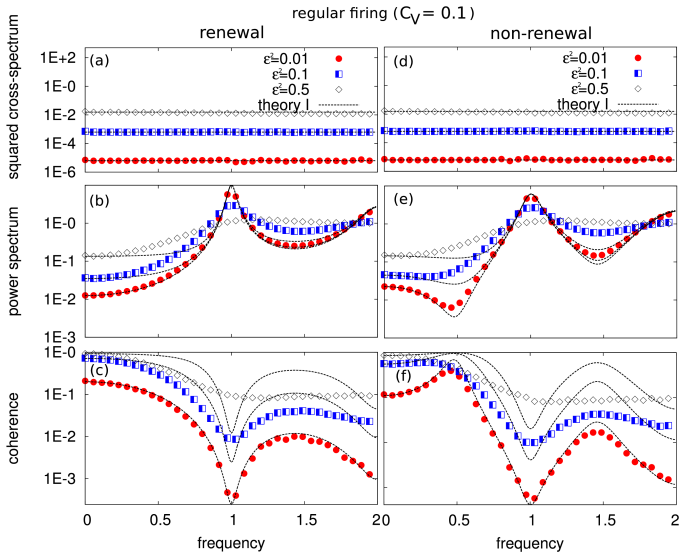

FIGURE 3. **Spectral measures for low intrinsic variability ($C_V = 0.1$) and different values of the signal strength using theory I, Eq.(18).** Comparison of squared spectrum (a,d), spike train power spectrum (b,d), and coherence (c,f) to theoretical predictions for the renewal model (left) and the non-renewal model (right).

II, based on Eq.(19) for the power spectrum, reproduces the simulation data quite well. In the following, we explore how robust the band-pass filter effect is and how well the two theories can describe spectrum and coherence for different intrinsic variability (different CVs) and different values of the signal amplitude (different values of ε).

3.2. **Dependence of information transmission on signal amplitude and intrinsic variability.** In Fig. 3 we compare the spectral statistics considered before for different values of the stimulus amplitude and for a low value of the spontaneous CV, implying a low intrinsic variability of the model. In this figure we use theory I for calculating the power spectrum and the coherence function. Because this theory holds true for weak stimuli only, power spectrum and coherence agree reasonably well with numerical simulations for a very small amplitude of $\varepsilon^2 = 0.01$. For this value, the band-pass filter effect is also most pronounced, i.e. the coherence in Fig. 3f has a pronounced peak around $f = 1/2$, corresponding to half the firing rate r_0. In contrast to this, the corresponding coherence function for the renewal model (Fig. 3c) attains its global maximum at zero frequency.

By increasing the signal amplitude, the coherence for both renewal and nonrenewal models attains the shape of a low-pass information filter and its overall amplitude increases significantly. At the same time the agreement with the simple theory becomes worse. This is due to the broadening of peaks in the spike-train power spectra, which become increasingly similar for renewal and non-renewal model. With

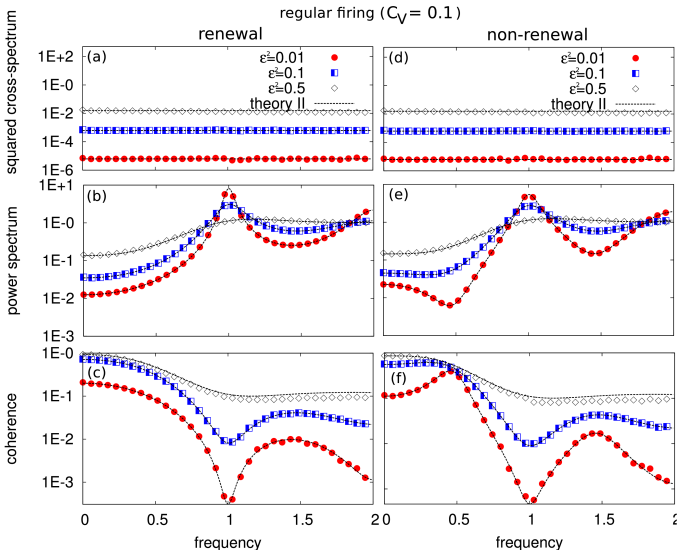

FIGURE 4. **Spectral measures for regular firing and different values of the signal strength using theory II, Eq.(19).** Comparison of squared spectrum (a,d), spike train power spectrum (b,d), and coherence (c,f) to theoretical predictions for the renewal model (left) and the non-renewal model (right).

a strong signal, the kind of reset does not matter anymore for the spiking statistics because the external signal "noise" (common to both renewal and non-renewal models) completely dominates the dynamics.

In Fig. 4 we show the same simulation data together with theoretical results using theory II for the power spectrum and the coherence function. The involved convolution-like expression in Eq.(19) captures the power spectrum and the resulting coherence function in an excellent manner even for comparatively strong stimulation. Theory II can thus describe faithfully how the information filtering effect due to positive ISI correlations is diminished and eventually destroyed for growing amplitude of the signal. We reiterate that this is expected because in the limit of strong external signal any feature of the intrinsic (spontaneous) dynamics is eliminated. In particular we expect for high cut-off frequency of the stimulus (i.e. an almost perfect white-noise stimulus) that the positive ISI correlations vanish for strong stimulation. This is just another manifestation of the fact that the two models do not differ anymore in this limit.

What is a weak signal? This depends a lot on the amount of intrinsic variability, as demonstrated in Fig. 5, where we show the same spectral statistics as before but for a spontaneous CV of 0.5 instead of 0.1. For such an intermediate level of the intrinsic variability, we illustrate in Fig. 5 that band-pass filtering of information is robust (see panel f), i.e. a maximum at non-vanishing frequency is observed for all signal amplitudes in the non-renewal model. The renewal model (cf. Fig. 5c) still acts as a low-pass filter of information. In addition, we note that theory I in this case provides a reasonable approximation for the power spectrum and the coherence even for the largest amplitude of $\varepsilon^2 = 0.5$. The reason for this is that the intrinsic variability linearizes the dynamical response. Put differently, the inherent

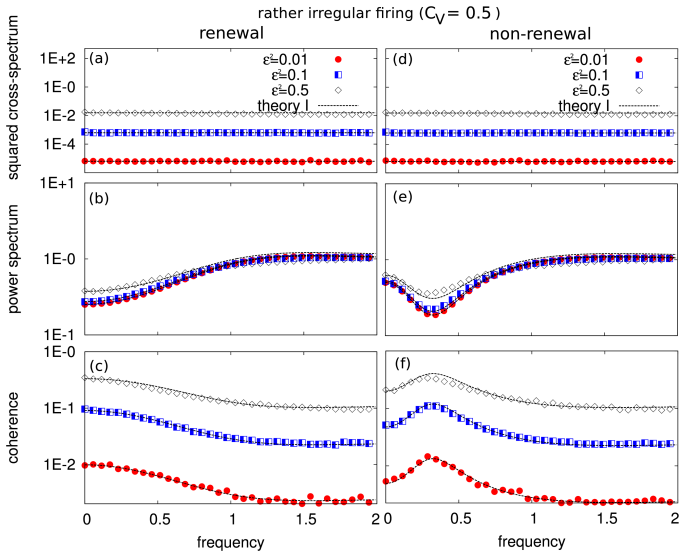

FIGURE 5. **Spectral measures for rather irregular firing and different values of the signal strength using theory I, Eq.(18).** Comparison of squared spectrum (a,d), spike train power spectrum (b,d), and coherence (c,f) to theoretical predictions for the renewal model (left) and the non-renewal model (right).

nonlinearity of resetting in the IF model is "washed out" by a sufficient amount of noise in the values of threshold and reset. As a consequence of this linearization, theory II yields only a minor improvement of the agreement between simulations and theory and is for this reason not shown here.

Finally, we discuss in Fig. 6 measures of information transmission and filtering as functions of the coefficient of variation in the presence of the stimulus. Note that this so-called evoked CV differs from the CV of the spontaneous activity (i.e. CV in the absence of a stimulus) that we used so far. For all data shown the evoked CV is varied by changing the spontaneous CV; both are connected by a monotonic relationship as demonstrated in Fig. 6d and h.

The statistics shown in Fig. 6a and b confirms what we already have seen in single coherence functions of the renewal model. For the entire range of the evoked CV the renewal model displays a clear low-pass filtering of information: the frequency $\hat{f}$ of the global coherence maximum is zero (Fig. 6a) and the quality is one (Fig. 6b). For the non-renewal model, we observe for most values of the CV a pronounced band-pass filtering of information with a frequency slightly below 0.5 (Fig. 6e), i.e. $\hat{f} \approx r_0/2$ (because, for all parameter sets, $r_0 = 1$). The extent of band-pass filtering in the non-renewal model depends in a non-trivial way on the spiking variability (CV) and on the signal amplitude (Fig. 6f). The largest value is achieved for a weak stimulus and low intrinsic variability. Note, that at this particular combination of ε and C_V the total information rate, Eq.(24), does not have to be maximal. Generally, the mutual information rate increases with signal amplitude and decreases with spike variability (here varied by increasing the threshold and reset variability). Both observations can be expected.

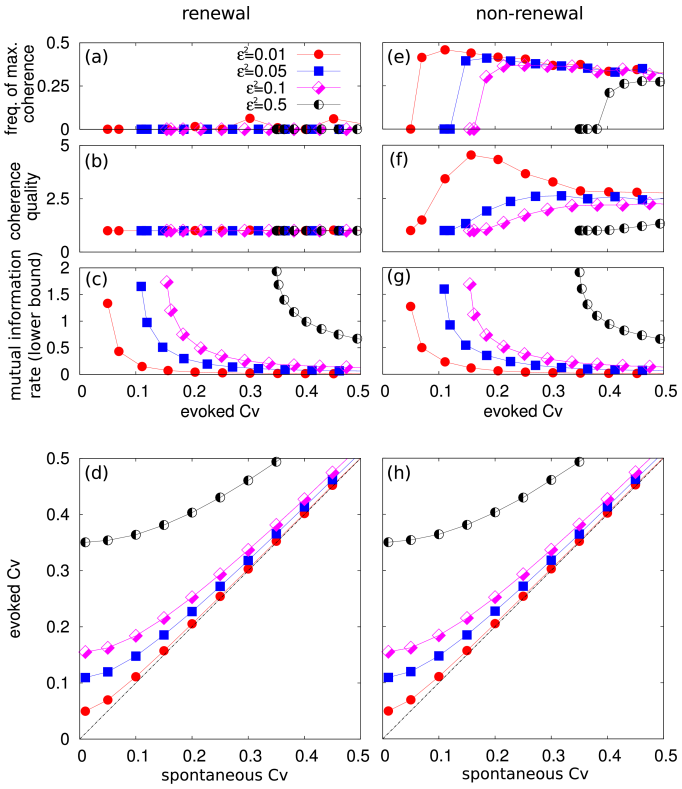

FIGURE 6. **Characteristics of the information transmission and filtering as functions of spiking variability for renewal model (left) and non-renewal model (right).** Shown are: frequency at which the coherence has its global maximum (a,e), quality of coherence, Eq.(23) (b,f), and lower bound on the mutual information rate, Eq.(24) (c,g). All statistics are determined from simulation data and plotted vs evoked coefficient of variation (CV in presence of broadband stimulus), which is also measured in simulations. The evoked CV was varied by changing the CV of the spontaneous activity, a parameter that enters the model through the distributions of threshold and reset, Eq.(6). Evoked CV is shown as a function of spontaneous CV in (d,h). All data are obtained from numerical simulations of the models.

3.3. **Analytical conditions for low-pass and band-pass filtering of information.** Even in the simple theory I the expressions for the coherence function are rather involved and it seems infeasible to determine the global maximum of the coherence analytically. As an approximate way to quantify band-pass filtering of information - or rather the deviation from low-pass filtering - we expand the coherence at low frequencies to second order

$$C_I(f) \approx C_I(0) + C_I^{(2)}(0)\frac{f^2}{2}. \tag{27}$$

Note that the coherence is an even function and therefore all odd derivatives vanish at zero frequency. Furthermore, with a view on Fig. 2c it seems justified to use theory I for the coherence at low frequencies where its agreement with simulations is better than around the maximum of the coherence function.

We can take the second derivative of the coherence, $C_I^{(2)}(0)$, its curvature, as a proxy for information filtering. If the curvature is positive, the coherence does not have a global maximum at zero frequency, i.e. it is not a low-pass filter. If the curvature is negative, it is an indication that the information transmission drops with increasing frequency, which is the hallmark of a low-pass filter of information. It is clear that with this locally defined measure we cannot make strict statements about global maxima of a function. However, specifically in our system we have observed numerically that the curvature at zero frequency is a reliable indicator of the filtering properties.

How can we calculate $C_I^{(2)}(0)$? Because the only frequency dependence of the coherence arises from the power spectrum, in the approximation of theory I determined by $C_I(f) \sim S_0^{-1}(f)$, the curvature can be expressed by the spontaneous power spectrum and its derivatives, $S_0(0), S_0^{(1)}(0), S_0^{(2)}(0)$. The latter in turn are related to the derivatives of the ISI's characteristic function at zero frequency, which are given by the moments of the ISI in the absence of a stimulus according to

$$\frac{d^n}{df^n}\tilde{F}_{1,0}(f)|_{f=0} = (2\pi i)^n \langle T^n \rangle. \tag{28}$$

Using this approach and applying it to the renewal and non-renewal models employing the expressions for the spontaneous power spectra, Eq.(14) and Eq.(15), we can express the curvature of the coherence at zero frequency by the moments of the ISI. For sake of simplicity we use the abbreviation $\mu_n =< T^n >$ (not to be confused with the base current μ of our models).

For the renewal model we obtain

$$C_{\mathrm{R}}^{(2)}(0) = \frac{2\pi^2 r_0^3 \varepsilon^2}{6 f_c \mu^2} \frac{3\mu_2^3 - 4\mu_1\mu_2\mu_3 + \mu_1^2\mu_4}{\left(r_0\mu_2 + \mu_1^2\left(r_0^2\varepsilon^2/(2f_c\mu^2) - r_0\right)\right)^2}. \tag{29}$$

The sign of the curvature is determined by the numerator of the fraction, i.e.

$$\begin{aligned} \mathrm{sign}\left(C_{\mathrm{R}}^{(2)}(0)\right) &= \mathrm{sign}\left(3\mu_2^3 - 4\mu_1\mu_2\mu_3 + \mu_1^2\mu_4\right), \\ &= \mathrm{sign}\left(-1 - (3+\beta_2)\, C_V^2 - 4\beta_1 C_V^3 + 3C_V^4\right). \end{aligned} \tag{30}$$

In the last line we expressed the moments in terms of the coefficient of variation (C_V), the skewness (β_1), and the kurtosis (β_2) (cf. Eq.(41) in the appendix, sec. (4)). ¿From these expressions that are valid for any distributions of threshold and reset we can conclude that for low spike variability ($C_V \to 0$) the renewal model acts as a low-pass filter because in this limit $\mathrm{sign}\left(C_{\mathrm{R}}^{(2)}(0)\right) \to \mathrm{sign}(-1)$. For the inverse Gaussian probability density skewness and kurtosis can be expressed by the C_V only (c.f. Eq.(43) in the appendix, sec. (4)), which yields

$$\mathrm{sign}\left(C_{\mathrm{R}}^{(2)}(0)\right) = \mathrm{sign}\left(-1 + 6C_{\mathrm{V}}^4\right). \tag{31}$$

Hence, the analytical condition for low-pass information filtering in the renewal model reads

$$C_{\mathrm{V}} < C_{\mathrm{V,crit}} = (1/6)^{1/4} \approx 0.6389. \tag{32}$$

If the C_V of the spontaneous activity in the renewal process is below the critical value $C_{\mathrm{V,crit}}$, the model will act as a low-pass filter of information, while higher values imply (a mild form of) band-pass filtering, which is also observed in simulations (not shown).

Using the same approach in the non-renewal model leads to expressions of comparable simplicity as in the renewal case. The curvature of the coherence for the non-renewal model is given by

$$C^{(2)}_{\mathrm{NR}}(0) = \frac{8\pi^2 r_0^3 \varepsilon^2}{6 f_c \mu^2} \frac{\left(3\mu_2^3 - 4\mu_1\mu_2\mu_3 + \mu_1^2\mu_4 - 3\mu_1^2\mu_2^2 - 3\mu_1^3\mu_3\right)}{\left(r_0\mu_2 + \mu_1^2\left(r_0^2\varepsilon^2/(2f_c\mu^2) - 2r_0\right)\right)^2}. \tag{33}$$

Again the sign of the curvature is determined by the numerator leading to

$$\begin{aligned} \operatorname{sign}\left(C^{(2)}_{\mathrm{NR}}(0)\right) &= \operatorname{sign}\left(3\mu_2^3 - 4\mu_1\mu_2\mu_3 + \mu_1^2\mu_4 - 3\mu_1^2\mu_2^2 - 3\mu_1^3\mu_3\right). \\ &= \operatorname{sign}\left(2 + 3\beta_1 C_V + (\beta_2 - 6) C_V^2 - 4\beta_1 C_V^3 + 3C_V^4\right) \end{aligned} \tag{34}$$

In the last line we expressed the moments by the higher cumulants. Here we can already detect an important difference to the renewal case: in the limit of low spiking variability, $C_{\mathrm{V}} \to 0$, the curvature becomes positive. For the inverse Gaussian probability density used in our model the curvature Eq.(34) can be further simplified

$$\operatorname{sign}\left(C^{(2)}_{\mathrm{NR}}(0)\right) = \operatorname{sign}\left(2 + 6C_{\mathrm{V}}^2 + 12C_{\mathrm{V}}^4\right). \tag{35}$$

Thus, the curvature is for all values of the C_{V} positive, which implies a band-pass filter of information in the non-renewal case irrespective of the spiking variability as long as the model operates in the linear-response regime.

4. Summary and discussion.

In this paper we have studied two simple integrate-and-fire model neurons with noise in the threshold and reset values. The statistical distributions of threshold and reset were for both models chosen as an inverse Gaussian probability density, such that the resulting ISI density of the IF model has also the form of an inverse Gaussian, a simple statistical distribution that fits the ISI density of some neurons surprisingly well [21, 17]. The two models differ in their reset rule, leading to the statistical independence of ISIs (renewal model) or to a positive correlation between adjacent ISIs (non-renewal model). By comparing the signal transmission of an additional time-dependent current stimulus in both models we could describe the effect of positive ISI correlations on information transmission.

Both models were simple enough to admit the derivation of analytical expressions or at least reasonable approximations for spectral measures that characterize neural information transmission. The most important measure was the spike train power spectrum that is strongly shaped by the absence or presence of positive ISI correlations. Because of its special relevance for our problem we applied two different approximations (previously developed in [28]) for the power spectrum in the presence of the broadband stimulus. In particular theory II by [28] showed a good agreement to numerical simulations for a wide range of signal amplitudes and different values of the intrinsic variability as quantified by the CV.

Our analytical and numerical results demonstrated unequivocally that positive ISI correlations reduce the coherence at low frequencies and increase it at intermediate frequencies. Positive ISI correlations imply an autonomous long-term variability, which is not related to the signal and which shapes the background noise spectrum such that noise power is shifted from higher frequencies to low frequencies. The

result is a band-pass information filter that does not necessarily transmit less information than its renewal counter part (cf. Fig. 6c and g). Our study has furthermore shown, that the effect is most pronounces for weak stimuli (where the simpler theory I provides a sufficient description of power spectrum and coherence), whereas for stronger stimulation the external signal dominates the spike train power spectrum such that differences between renewal and non-renewal models become small.

For our simple models and in the limit of weak stimulation we could derive explicit expressions for the curvature of the coherence (using the simpler theory I from Ref. [28]). These allowed us to formulate precise conditions for having a local maximum (negative curvature) or minimum (positive curvature) of the coherence at zero frequency, which can be regarded as a proxy for low-pass or high-pass filtering of information, respectively. Indeed, for values of the coefficient of variation between 0 and 1/2 the renewal model always displays a negative curvature and, in line with this, the global maximum of the coherence is attained at zero frequency, similar to the case of nonlinear IF models with more realistic current noise [51]. The non-renewal model possesses always a positive curvature at $f = 0$ and a global maximum at non-vanishing frequency.

The non-renewal model inspected in this paper is still limited to exclusive correlations between adjacent intervals. It remains an open question whether threshold and reset rules could be generalized to obtain a model with ISI correlations that extend beyond lag one and in which spectral measures can still be analytically calculated. Apart from such abstract generalizations, it would also be of interest to explore the information-filtering effects of positive ISI correlations in biophysically more realistic neuron models. As mentioned in the introduction, positive ISI correlations can arise from different sources: external stimulation, intrinsic channel noise, or subthreshold adaptation. We expect that the noise-shaping effect discussed for our simple model will also emerge in biophysical models that incorporate the sources of nonrenewal behavior directly. Whether the information-filtering effect in a more realistic model is more or less pronounced than in our setup can only be revealed in future studies.

Acknowledgments. SB and BL were supported by the Bundesministerium für Bildung und Forschung (FKZ:01GQ1001A). BL wants to thank Maurice Chacron (McGill University, Montréal, Canada) for an inspiring discussion on the topic of this paper.

Appendix.

Spontaneous power spectrum of the non-renewal model. According to Eq.(13) the power spectrum of a stationary point process can be calculated if we know the characteristic functions of the T_n (the n-th order intervals defined as the sum of n subsequent ISIs). These are the Fourier transforms $\tilde{F}_n(f)$ of the probability densities $F_n(T_n)$. In the non-renewal model, the n-th order interval can be regarded as the sum of $2n$ sub-intervals that go from reset to zero, $\hat{\tau}_i$, and from zero to threshold, τ_i, respectively (see Fig. 7). Note that the non-renewal ISI sequence is equivalent to a moving average process of order one; for results on such processes (some of which are derived below for completeness), see for instance [23].

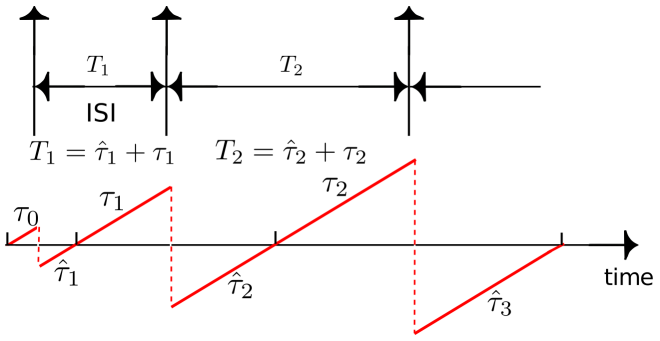

FIGURE 7. **Subdivision of the ISIs into sub-intervals.**

Many of these sub-intervals are pairwise identical because of the mirroring rule ($\tau_i = \hat{\tau}_{i+1}$), leading to the following expression:

$$T_n = \hat{\tau}_1 + \tau_1 + \hat{\tau}_2 + \tau_2 + \cdots + \hat{\tau}_n + \tau_n = \tau_0 + \tau_n + 2\sum_{j=1}^{n-1} \tau_j. \tag{36}$$

In the last step we have expressed T_n by a sum of independent variables, the probability density of which is given by the convolution of the probability densities of the single variables and the characteristic function of which is given by the product of the single characteristic functions

$$\tilde{F}_n = \tilde{F}_\tau(f)^2 \tilde{F}_{2\tau}(f)^{n-1} = \tilde{F}_\tau(f)^2 \tilde{F}_\tau(2f)^{n-1}, \tag{37}$$

where we used $\tilde{F}_{2\tau}(f) = \tilde{F}_\tau(2f)$. Inserting this for $\tilde{F}_n$ in the general formula Eq.(13) and simplifying the resulting geometric series, we end up with the analytical expression for the spike train power spectrum of the non-renewal model in the spontaneous case

$$S_{\mathrm{NR},0}(f)/r_0 = \\ = \frac{\left|1 - \sqrt{\tilde{F}_{1,0}(2f)}\right|^2 + \tilde{F}_{1,0}(f)\left(1 - \sqrt{\tilde{F}_{1,0}(2f)}\right)^* + \tilde{F}^*_{1,0}(f)\left(1 - \sqrt{\tilde{F}_{1,0}(2f)}\right)}{\left|1 - \sqrt{\tilde{F}_{1,0}(2f)}\right|^2}, \tag{38}$$

which can be further simplified to Eq.(15). This result holds true with arbitrary distributions of threshold and reset. It is easily evaluated for the case of the inverse Gaussian considered in this paper, for which the Fourier transform is given in Eq.(16).

Serial correlation coefficient of the non-renewal model. We use the same subdivision of ISIs as in the previous subsection and write the covariance between two intervals T_i and T_{i+k} as follows

$$\langle \Delta T_i \Delta T_{i+k} \rangle = \langle T_i T_{i+k} \rangle - \langle T_i \rangle \langle T_{i+k} \rangle = \langle (\tau_{i-1} + \tau_i)(\tau_{i+k} + \tau_{i+1+k}) \rangle - \langle (\tau_{i-1} + \tau_i) \rangle^2, \tag{39}$$

where all the τ_i are statistically independent and identically distributed variables. It is simple to show that this covariance vanishes for $k > 1$. For $k = 1$ we obtain

$$\langle \Delta T_i \Delta T_{i+k} \rangle = 3\langle \tau \rangle^2 + \langle \tau^2 \rangle - 4\langle \tau \rangle^2 = \langle \Delta \tau^2 \rangle = \frac{\langle \Delta T^2 \rangle}{2}, \tag{40}$$

which results in the serial correlation coefficient stated in Eq.(9), a well-known result from the literature on moving-average processes [23, 7].

Raw and standardized moments of the inverse Gaussian ISI density. Skewness β_1 and kurtosis β_2 as used in the main text are related to the raw moments $\mu_n = \langle T^n \rangle$ by

$$\begin{aligned} \beta_1 &= \frac{\mu_3 - 3\mu_1\left(\mu_2 - \mu_1^2\right) - \mu_1^3}{\left(\mu_2 - \mu_1^2\right)^{3/2}}, \\ \beta_2 &= \frac{\mu_4 - 4\mu_1\mu_3 + 6\mu_1^2\mu_2 - 3\mu_1^4}{\mu_1^4 - 2\mu_1^2\mu_2 + \mu_2^2}. \end{aligned} \tag{41}$$

For an inverse Gaussian probability density given in Eq.(5), the moments read as follows

$$\begin{aligned} \mu_1 &= 1/r_0, \quad \mu_2 = \left(1 + C_{\mathrm{V}}^2\right)/r_0^2, \\ \mu_3 &= \left(1 + 3C_{\mathrm{V}}^2 + 3C_{\mathrm{V}}^4\right)/r_0^3, \quad \mu_4 = \left(1 + 3C_{\mathrm{V}}^2 + 15C_{\mathrm{V}}^4 + 15C_{\mathrm{V}}^6\right)/r_0^4, \end{aligned} \tag{42}$$

while skewness and kurtosis are given by

$$\beta_1 = 3C_{\mathrm{V}}, \quad \beta_2 = 3 + C_{\mathrm{V}}^2. \tag{43}$$

REFERENCES

[1] L. F. Abbott and W. G. Regehr, Synaptic computation, *Nature,* **431** (2004), 796–803.

[2] R. Azouz and C. M. Gray, Dynamic spike threshold reveals a mechanism for synaptic coincidence detection in cortical neurons in vivo, *Proc. Nat. Acad. Sci.,* **97** (2000), 8110–8115.

[3] D. Bernardi and B. Lindner, A frequency-resolved mutual information rate and its application to neural systems, *J. Neurophysiol.,* **113** (2014), 1342–1357.

[4] S. Blankenburg, W. Wu, B. Lindner and S. Schreiber, Information filtering in resonant neurons, *J. Comput. Neurosci.*, **39** (2015), 349–370.

[5] A. Borst and F. Theunissen, Information theory and neural coding, *Nat. Neurosci.,* **2** (1999), 947–957.

[6] N. Brenner, O. Agam, W. Bialek and R. de Ruyter van Steveninck, Statistical properties of spike trains: Universal and stimulus-dependent aspects, *Phys. Rev. E,* **66** (2002), 031907, 14pp.

[7] P. J. Brockwell and R. A. Davis, *Time Series: Theory and Methods*, Springer, 2009.

[8] N. Brunel, V. Hakim and M. J. E. Richardson, Firing-rate resonance in a generalized integrate-and-fire neuron with subthreshold resonance, *Phys. Rev. E,* **67** (2003), 051916, 23pp.

[9] M. Chacron, B. Lindner and A. Longtin, Threshold fatigue and information transfer, *J. Comput. Neurosci.,* **23** (2007), 301–311.

[10] M. J. Chacron, A. Longtin and L. Maler, Negative interspike interval correlations increase the neuronal capacity for encoding time-dependent stimuli, *J. Neurosci.,* **21** (2001), 5328–5343.

[11] M. J. Chacron, B. Doiron, L. Maler, A. Longtin and J. Bastian, Non-classical receptive field mediates switch in a sensory neuron's frequency tuning, *Nature,* **423** (2003), 77–81.

[12] M. J. Chacron, B. Lindner and A. Longtin, Noise shaping by interval correlations increases information transfer, *Phys. Rev. Lett.,* **93** (2004), 059904.

[13] T. Cover and J. Thomas, *Elements of Information Theory*, Wiley, New-York, 1991.

[14] D. R. Cox and P. A. W. Lewis, *The Statistical Analysis of Series of Events*, Chapman and Hall, London, 1966.

[15] F. Droste, T. Schwalger and B. Lindner, Interplay of two signals in a neuron with short-term synaptic plasticity, *Front. Comp. Neurosci.,* **7** (2013), p86.

[16] T. A. Engel, L. Schimansky-Geier, A. V. M. Herz, S. Schreiber and I. Erchova, Subthreshold membrane-potential resonances shape spike-train patterns in the entorhinal cortex, *J. Neurophysiol.,* **100** (2008), 1576–1589.

[17] K. Fisch, T. Schwalger, B. Lindner, A. Herz and J. Benda, Channel noise from both slow adaptation currents and fast currents is required to explain spike-response variability in a sensory neuron, *J. Neurosci.,* **32** (2012), 17332–17344.

[18] J. L. Folks and R. S. Chhikara, The inverse gaussian distribution and its statistical application-a review, *J. R. Statist. Soc. B,* **40** (1978), 263–289.
[19] F. Gabbiani, Coding of time-varying signals in spike trains of linear and half-wave rectifying neurons, *Network Comp. Neural.,* **7** (1996), 61–85.
[20] C. D. Geisler and J. M. Goldberg, A stochastic model of repetitive activity of neurons, *Biophys. J.,* **6** (1966), 53–69.
[21] G. L. Gerstein and B. Mandelbrot, Random walk models for the spike activity of a single neuron, *Biophys. J.,* **4** (1964), 41–68.
[22] W. Gerstner and W. M. Kistler, *Spiking Neuron Models*, Cambridge University Press, Cambridge, 2002.
[23] J. D. Hamilton, *Time Series Analysis*, Princeton University Press, 1994.
[24] A. V. Holden, *Models of the Stochastic Activity of Neurones*, Springer-Verlag, Berlin, 1976.
[25] E. M. Izhikevich, Resonate-and-fire neurons, *Neural. Netw.,* **14** (2001), 883–894.
[26] B. Lindner, Interspike interval statistics of neurons driven by colored noise, *Phys. Rev. E,* **69** (2004), 022901.
[27] B. Lindner, Low-pass filtering of information in the leaky integrate-and-fire neuron driven by white noise, in *International Conference on Theory and Application in Nonlinear Dynamics (ICAND 2012)* (eds. I. Visarath, A. Palacios and P. Longhini), Springer, 2012.
[28] B. Lindner, M. J. Chacron, A. Longtin, Integrate-and-fire neurons with threshold noise - a tractable model of how interspike interval correlations affect neuronal signal transmission, *Phys. Rev. E,* **72** (2005), p021911, 21pp.
[29] B. Lindner, D. Gangloff, A. Longtin and J. E. Lewis, Broadband coding with dynamic synapses, *J. Neurosci.,* **29** (2009), 2076–2087.
[30] S. B. Lowen and M. C. Teich, Auditory-nerve action potentials form a nonrenewal point process over short as well as long time scales, *J. Acoust. Soc. Am.,* **92** (1992), 803–806.
[31] D. J. Mar, C. C. Chow, W. Gerstner, R. W. Adams and J. J. Collins, Noise shaping in populations of coupled model neurons, *Proc. Natl. Acad. Sci.,* **96** (1999), 10450–10455.
[32] G. Marsat and G. S. Pollack, Differential temporal coding of rhythmically diverse acoustic signals by a single interneuron, *J. Neurophysiol.,* **92** (2004), 939–948.
[33] C. Massot, M. Chacron and K. Cullen, Information transmission and detection thresholds in the vestibular nuclei: Single neurons vs. population encoding, *J. Neurophysiol.,* **105** (2011), 1798–1814.
[34] M. Merkel and B. Lindner, Synaptic filtering of rate-coded information, *Phys. Rev. E,* **81** (2010), 041921, 19pp.
[35] J. W. Middleton, A. Longtin, J. Benda and L. Maler, Postsynaptic receptive field size and spike threshold determine encoding of high-frequency information via sensitivity to synchronous presynaptic activity, *J. Neurophysiol.,* **101** (2009), 1160–1170.
[36] A. B. Neiman and D. F. Russell, Sensory coding in oscillatory electroreceptors of paddlefish, *Chaos,* **21** (2011), 047505.
[37] A. Nikitin, N. Stocks and A. Bulsara, Enhancing the resolution of a sensor via negative correlation: A biologically inspired approach, *Phys. Rev. Lett.,* **109** (2012), 238103.
[38] A. M. M. Oswald, M. J. Chacron, B. Doiron, J. Bastian and L. Maler, Parallel processing of sensory input by bursts and isolated spikes, *J. Neurosci.,* **24** (2004), 4351–4362.
[39] S. A. Prescott and T. J. Sejnowski, Spike-rate coding and spike-time coding are affected oppositely by different adaptation mechanisms, *J. Neurosci.,* **28** (2008), 13649–13661.
[40] F. Rieke, D. Bodnar and W. Bialek, Naturalistic stimuli increase the rate and efficiency of information transmission by primary auditory afferents, *Proc. Biol. Sci.,* **262** (1995), 259–265.
[41] F. Rieke, D. Warland, R. de Ruyter van Steveninck and W. Bialek, *Spikes: Exploring the Neural Code*, MIT Press, Cambridge, Massachusetts, 1999.
[42] J. C. Roddey, B. Girish and J. P. Miller, Assessing the performance of neural encoding models in the presence of noise, *J. Comput. Neurosci.,* **8** (2000), 95–112.
[43] S. G. Sadeghi, M. J. Chacron, M. C. Taylor and K. E. Cullen, Neural variability, detection thresholds, and information transmission in the vestibular system, *J. Neurosci.,* **27** (2007), 771–781.
[44] T. Schwalger, K. Fisch, J. Benda and B. Lindner, How noisy adaptation of neurons shapes interspike interval histograms and correlations, *PLoS Comp. Biol.,* **6** (2010), e1001026, 25pp.
[45] R. Shannon, The mathematical theory of communication, *Bell Syst. Tech. J.,* **27** (1948), 379–423.

[46] N. Sharafi, J. Benda and B. Lindner, Information filtering by synchronous spikes in a neural population, *J. Comp. Neurosci.,* **34** (2013), 285–301.
[47] L. Shiau, T. Schwalger and B. Lindner, ISI correlation in a stochastic exponential integrate-and-fire model with subthreshold and spike-triggered adaptation, *J. Comp. Neurosci.,* **38** (2015), 589–600.
[48] J. Shin, The noise shaping neural coding hypothesis: A brief history and physiological implications, *Neurocomp.,* **44** (2002), 167–175.
[49] J. H. Shin, K. R. Lee and S. B. Park, Novel neural circuits based on stochastic pulse coding and noise feedback pulse coding, *Int. J. Electronics,* **74** (1993), 359–368.
[50] R. L. Stratonovich, *Topics in the Theory of Random Noise*, Gordon and Breach, New York, 1967.
[51] R. D. Vilela and B. Lindner, Comparative study of different integrate-and-fire neurons: Spontaneous activity, dynamical response, and stimulus-induced correlation, *Phys. Rev. E,* **80** (2009), 031909.
[52] R. S. Zucker and W. G. Regehr, Short-term synaptic plasticity, *Ann. Rev. Physiol.,* **64** (2002), 355–405.

Received April 01, 2015; Accepted June 21, 2015.

E-mail address: sven.blankenburg@physik.hu-berlin.de
E-mail address: benjamin.lindner@physik.hu-berlin.de